Digital Redesign of an Optimal Momentum Management Controller for the Space Station

J. W. Sunkel
NASA Johnson Space Center, Houston, Texas 77058
and
L. S. Shieh and J. L. Zhang
University of Houston, Houston, Texas 77204

A digital redesign technique is developed for determining the digital version of an optimal momentum management controller previously designed by the authors for the Space Station Freedom. The technique matches the continuous-time and discrete-time states at all sampling instants to find a pseudocontinuous-time quadratic regulator from a continuous-time quadratic regulator. It is shown that the redesigned digital states closely match the continuous-time optimal states. It is also shown that the digital redesigned state-feedback control law based on the bilinear transformation method is a class of the proposed control law. The digital redesign technique is then extended to find the digital version of the continuous-time optimal observer. It is shown that the states of the redesigned digital observer closely match those of the continuous-time optimal observer.

I. Introduction

THE Space Station Freedom (Fig. 1) will employ a distributed system of microprocessors to perform all flight operations. This means that a digital control law is required for the momentum management and attitude control of the Station. Therefore, the necessity arises for either designing a digital momentum management controller or converting an existing analog controller into a digital control law. Since a digitized continuous-time system with a very small sampling period may become an unstable and/or nonminimum phase model[1-3] even if the original continuous-time system is stable and/or minimum phase, the direct digital design of the contin-

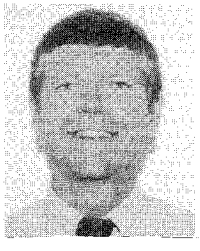

John W. Sunkel received his B.S. and M.S. degrees in Aerospace Engineering from the University of Colorado, Boulder, CO, and his Ph.D. in Systems Engineering from the University of Houston, Houston, TX. He has been with NASA Johnson Space Center since 1965 and has been involved in a number of major programs including development of both the ascent and return to launch site abort autopilots for the Space Shuttle and, more recently, the Solar Array Flight experiment. He is currently responsible for the integration and development of the attitude control system for Space Station Freedom.

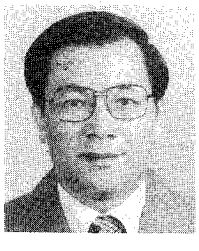

Leang-San Shieh received his B.S. degree from the National Taiwan University, Taiwan, in 1958, and his M.S. and Ph.D. degrees from the University of Houston, Houston, TX, in 1968 and 1970, respectively, all in Electrical Engineering. He joined the Department of Electrical Engineering at the University of Houston in 1971 as an assistant professor and was promoted to associate professor in 1974, and professor in 1978. Dr. Shieh is a member of AIAA and IEEE and a Registered Professional Engineer in the State of Texas. He was a recipient of the 1973 College Teaching Excellence Award and the 1988 College Research Excellence Award from the Cullen College of Engineering, University of Houston, and the 1976 University Teaching Excellence Award from the University of Houston. Further, he received the Honor of Merit from Instituto Universitario Politecnico, Republic of Venezuela in 1978. His fields of interest are control systems, optimal control, adaptive digital control, and large-scale systems. He has published more than 100 articles in various scientific journals. He coauthored a research monograph, *An Algebraic Approach to Structural Analysis and Design of Multivariable Control Systems* (Springer, New York) in 1988.

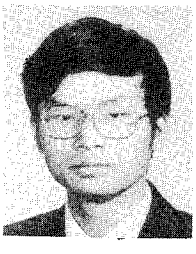

Jianliang Zhang received his B.S. and M.S. degrees in Electrical Engineering from the Kunming Institute of Technology, China, in 1982 and the University of Houston, Houston, TX, in 1988, respectively. He was a faculty member at the Kunming Institute of Technology between 1982 and 1986. At present, he is working toward his Ph.D. degree in the field of Digital Control System Theory at the University of Houston, Houston, TX.

Presented as Paper 89-3473 at the AIAA Guidance, Navigation, and Control Conference, Boston, MA, Aug. 14-16, 1989; received April 2, 1990; revision received July 25, 1990; accepted for publication July 25, 1990. Copyright © 1990 by the American Institute of Aeronautics and Astronautics, Inc. No copyright is asserted in the United States under Title 17, U.S. Code. The U.S. Government has a royalty-free license to exercise all rights under the copyright claimed herein for Governmental purposes. All other rights are reserved by the copyright owner.

uous-time Space Station in the discrete-time domain is not closely coupled with the continuous aspects of the real system. Moreover, effective optimal regional-pole placement techniques[4,5] are not available in digital control theory[1-3]; hence, the responses of the directly digitally designed continuous-time Space Station may be undesirable. In this paper, we have elected to convert an existing analog optimal momentum management controller previously designed by the authors[4] into an equivalent digital controller. For digital implementation of the designed continuous-time controller, the continuous-time controller must be converted into an equivalent digital controller. This is called a digital redesign problem.[1] Based on matching all the states of a continuous-time system and an equivalent discrete-time system[1,6,7] (Fig. 2), a digital redesign technique is presented for finding the equivalent digital optimal momentum management controller.

As a further illustration of the digital redesign technique, we show that the same approach taken in Ref. 4 can be used to design a continuous-time optimal observer for the Space Station. That approach combines the regional pole assignment method[6,7] and optimal control techniques[8] to determine a unique set of feedback gains for the continuous-time optimal observer. To limit the closed-loop bandwidth of the designed observer to reduce the effects of high-frequency disturbances on the observer and to insure proper and quick convergence of the estimated states to the original states, we design the optimal observer so that the closed-loop eigenvalues of the observer will be optimally placed within a specified vertical strip on the negative real axis in the left half s plane. Then, taking this continuous-time optimal observer, we show how the digital redesign technique can be used to find the digital version.

II. Mathematical Models for Momentum Management of the Space Station

The Space Station in circular orbit is expected to maintain local vertical and local horizontal (LVLH) orientation during normal mode operation. The nonlinear equations of motion in terms of components along the body-fixed control axes can be written as the following[4,9]:

Space Station Dynamics ($J_{ij} = J_{ji}$ for $i \neq j$):

$$\begin{bmatrix} J_{11} & J_{12} & J_{13} \\ J_{21} & J_{22} & J_{23} \\ J_{31} & J_{32} & J_{33} \end{bmatrix} \begin{bmatrix} \dot{\omega}_1 \\ \dot{\omega}_2 \\ \dot{\omega}_3 \end{bmatrix} = - \begin{bmatrix} 0 & -\omega_3 & \omega_2 \\ \omega_3 & 0 & -\omega_1 \\ -\omega_2 & \omega_1 & 0 \end{bmatrix}$$

$$\times \begin{bmatrix} J_{11} & J_{12} & J_{13} \\ J_{21} & J_{22} & J_{23} \\ J_{31} & J_{32} & J_{33} \end{bmatrix} \begin{bmatrix} \omega_1 \\ \omega_2 \\ \omega_3 \end{bmatrix} + 3n^2 \begin{bmatrix} 0 & -c_3 & c_2 \\ c_3 & 0 & -c_1 \\ -c_2 & c_1 & 0 \end{bmatrix}$$

$$\times \begin{bmatrix} J_{11} & J_{12} & J_{13} \\ J_{21} & J_{22} & J_{23} \\ J_{31} & J_{32} & J_{33} \end{bmatrix} \begin{bmatrix} c_1 \\ c_2 \\ c_3 \end{bmatrix} + \begin{bmatrix} -u_1 + w_1 \\ -u_2 + w_2 \\ -u_3 + w_3 \end{bmatrix} \tag{1}$$

where

$$c_1 \triangleq -\sin\theta_2 \cos\theta_3 \tag{2a}$$

$$c_2 \triangleq \cos\theta_1 \sin\theta_2 \sin\theta_3 + \sin\theta_1 \cos\theta_2 \tag{2b}$$

$$c_3 \triangleq -\sin\theta_1 \sin\theta_2 \sin\theta_3 + \cos\theta_1 \cos\theta_2 \tag{2c}$$

Attitude Kinematics (2-3-1 body-axis sequence):

$$\begin{bmatrix} \dot{\theta}_1 \\ \dot{\theta}_2 \\ \dot{\theta}_3 \end{bmatrix} = \frac{1}{\cos\theta_3} \begin{bmatrix} \cos\theta_3 & -\cos\theta_1 \sin\theta_3 & \sin\theta_1 \sin\theta_3 \\ 0 & \cos\theta_1 & -\sin\theta_1 \\ 0 & \sin\theta_1 \cos\theta_3 & \cos\theta_1 \cos\theta_3 \end{bmatrix} \begin{bmatrix} \omega_1 \\ \omega_2 \\ \omega_3 \end{bmatrix} + \begin{bmatrix} 0 \\ n \\ 0 \end{bmatrix} \tag{3}$$

Control moment gyro (CMG) Momentum:

$$\begin{bmatrix} \dot{h}_1 \\ \dot{h}_2 \\ \dot{h}_3 \end{bmatrix} + \begin{bmatrix} 0 & -\omega_3 & \omega_2 \\ \omega_3 & 0 & -\omega_1 \\ -\omega_2 & \omega_1 & 0 \end{bmatrix} \begin{bmatrix} h_1 \\ h_2 \\ h_3 \end{bmatrix} = \begin{bmatrix} u_1 \\ u_2 \\ u_3 \end{bmatrix} \tag{4}$$

where (1,2,3) are the roll, pitch, and yaw control axes whose origin is fixed at the mass center, with the roll axis in the flight direction, the pitch axis perpendicular to the orbit plane, and the yaw axis toward the Earth; $(\theta_1,\theta_2,\theta_3)$ are the roll, pitch, and yaw Euler angles of the central (body) axes with respect to LVLH axes that rotate with the orbital angular velocity n; $(\omega_1,\omega_2,\omega_3)$ are the body-axis components of the absolute angular velocity of the station; (J_{11}, J_{22}, J_{33}) are the moments of inertia; $J_{ij} = J_{ji} (i \neq j)$ are the products of inertia; (h_1,h_2,h_3) are the body-axis components of the CMG momentum; (u_1,u_2,u_3) are the body-axis components of the control torque caused by the CMG momentum change; (w_1,w_2,w_3) are the body-axis components of the external disturbance torque; and n is the orbital rate of 0.0011 rad/s.

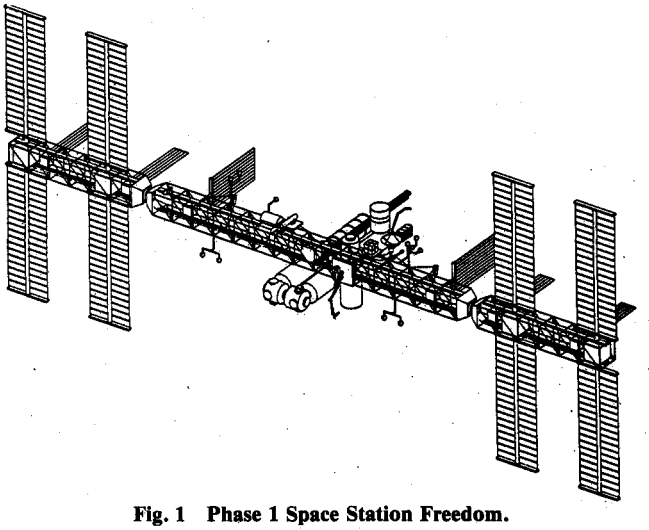

Fig. 1 Phase 1 Space Station Freedom.

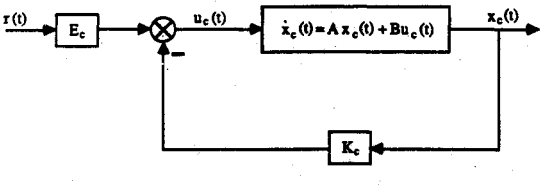

a) Continuous system

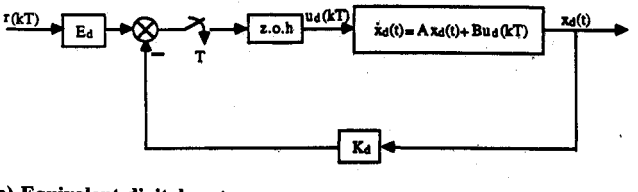

b) Equivalent digital system

Fig. 2 Block diagrams of the systems.

For small attitude deviations from LVLH orientation with an assumption that $n \gg |\Delta\omega_i|$, $i = 1,2,3$ where $\Delta\omega = [\omega_1, \omega_2 + n, \omega_3]^T$, the linearized equations of motion can be written as the following:

Space Station Dynamics ($J_{ij} = J_{ji}$ for $i \neq j$):

$$\begin{bmatrix} J_{11} & J_{12} & J_{13} \\ J_{21} & J_{22} & J_{23} \\ J_{31} & J_{32} & J_{33} \end{bmatrix} \begin{bmatrix} \dot{\omega}_1 \\ \dot{\omega}_2 \\ \dot{\omega}_3 \end{bmatrix} = n \begin{bmatrix} J_{31} & 2J_{32} & J_{33} - J_{22} \\ -J_{32} & 0 & J_{12} \\ J_{22} - J_{11} & -2J_{12} & -J_{13} \end{bmatrix}$$

$$\times \begin{bmatrix} \omega_1 \\ \omega_2 \\ \omega_3 \end{bmatrix} + 3n^2 \begin{bmatrix} J_{33} - J_{22} & J_{21} & 0 \\ J_{12} & J_{33} - J_{11} & 0 \\ -J_{13} & -J_{23} & 0 \end{bmatrix} \begin{bmatrix} \theta_1 \\ \theta_2 \\ \theta_3 \end{bmatrix}$$

$$+ n^2 \begin{bmatrix} -2J_{23} \\ 3J_{13} \\ -J_{12} \end{bmatrix} + \begin{bmatrix} -u_1 + w_1 \\ -u_2 + w_2 \\ -u_3 + w_3 \end{bmatrix} \tag{5}$$

Attitude Kinematics:

$$\dot{\theta}_1 - n\theta_3 = \omega_1 \tag{6a}$$

$$\dot{\theta}_2 - n = \omega_2 \tag{6b}$$

$$\dot{\theta}_3 + n\theta_1 = \omega_3 \tag{6c}$$

Since pitch motion is uncoupled from roll/yaw motion, pitch control is treated separately from coupled roll/yaw control.

Expected aerodynamic disturbances w_i are modeled as a bias plus cyclic terms in the body-fixed control axes:

$$w_i(t) = \text{bias} + A_n \sin(nt + \phi_n) + A_{2n} \sin(2nt + \phi_{2n}) \tag{9}$$

The cyclic component at orbital rate is due to the diurnal bulge effect, whereas the cyclic torque at twice the orbital rate is caused by the rotatory solar panels.

To avoid CMG momentum buildup, we introduce an integral of the CMG momentum vector $\boldsymbol{h}$, i.e.,

$$\hat{\boldsymbol{h}} = \int \boldsymbol{h}\, dt \qquad \text{or} \qquad \dot{\hat{\boldsymbol{h}}} = \boldsymbol{h} \tag{10}$$

Combining Eqs. (6-8) with Eq. (10), we obtain the state space representation to be used for the control design as

Pitch Axis:

$$\begin{bmatrix} \dot{\theta}_2 \\ \dot{\omega}_2 \\ \dot{h}_2 \\ \dot{\hat{h}}_2 \end{bmatrix} = \begin{bmatrix} 0 & 1 & 0 & 0 \\ 3n^2(J_3 - J_1)/J_2 & 0 & 0 & 0 \\ 0 & 0 & 0 & 0 \\ 0 & 0 & 1 & 0 \end{bmatrix} \begin{bmatrix} \theta_2 \\ \omega_2 \\ h_2 \\ \hat{h}_2 \end{bmatrix} + \begin{bmatrix} 0 \\ -1/J_2 \\ 1 \\ 0 \end{bmatrix} u_2 + \begin{bmatrix} 0 \\ 1/J_2 \\ 0 \\ 0 \end{bmatrix} w_2 \tag{11}$$

Roll/Yaw Axes:

$$\begin{bmatrix} \dot{\theta}_1 \\ \dot{\omega}_1 \\ \dot{h}_1 \\ \dot{\hat{h}}_1 \\ \dot{\theta}_3 \\ \dot{\omega}_3 \\ \dot{h}_3 \\ \dot{\hat{h}}_3 \end{bmatrix} = \begin{bmatrix} 0 & 1 & 0 & 0 & n & 0 & 0 & 0 \\ 3n^2(J_3 - J_2)/J_1 & 0 & 0 & 0 & 0 & n(J_3 - J_2)/J_1 & 0 & 0 \\ 0 & 0 & 0 & 0 & 0 & 0 & n & 0 \\ 0 & 0 & 1 & 0 & 0 & 0 & 0 & 0 \\ -n & 0 & 0 & 0 & 0 & 1 & 0 & 0 \\ 0 & n(J_2 - J_1)/J_3 & 0 & 0 & 0 & 0 & 0 & 0 \\ 0 & 0 & -n & 0 & 0 & 0 & 0 & 0 \\ 0 & 0 & 0 & 0 & 0 & 0 & 1 & 0 \end{bmatrix} \begin{bmatrix} \theta_1 \\ \omega_1 \\ h_1 \\ \hat{h}_1 \\ \theta_3 \\ \omega_3 \\ h_3 \\ \hat{h}_3 \end{bmatrix} + \begin{bmatrix} 0 & 0 \\ -1/J_1 & 0 \\ 1 & 0 \\ 0 & 0 \\ 0 & 0 \\ 0 & -1/J_3 \\ 0 & 1 \\ 0 & 0 \end{bmatrix} \begin{bmatrix} u_1 \\ u_3 \end{bmatrix} + \begin{bmatrix} 0 & 0 \\ 1/J_1 & 0 \\ 0 & 0 \\ 0 & 0 \\ 0 & 0 \\ 0 & 1/J_3 \\ 0 & 0 \\ 0 & 0 \end{bmatrix} \begin{bmatrix} w_1 \\ w_3 \end{bmatrix} \tag{12}$$

CMG Momentum:

$$\dot{h}_1 - nh_3 = u_1 \tag{7a}$$

$$\dot{h}_2 = u_2 \tag{7b}$$

$$\dot{h}_3 + nh_1 = u_3 \tag{7c}$$

The products of inertia cause three-axis coupling as well as a bias torque in each axis. Early flight configurations during station assembly may have significant misalignment of the control axes with the principal axes. In such cases, the previous linear, three-axis coupled equations of motion should be used for control design.

In this paper, we are concerned with the phase I assembly complete configuration. The small products of inertia permit pitch motion to be uncoupled from roll/yaw motion. For this case, the control axes are nearly aligned with the principal axes ($J_1 \triangleq J_{11}$, $J_2 \triangleq J_{22}$, and $J_3 \triangleq J_{33}$). Eq. (5) becomes

$$J_1\dot{\omega}_1 + n(J_2 - J_3)\omega_3 + 3n^2(J_2 - J_3)\theta_1 = -u_1 + w_1 \tag{8a}$$

$$J_2\dot{\omega}_2 + 3n^2(J_1 - J_3)\theta_2 = -u_2 + w_2 \tag{8b}$$

$$J_3\dot{\omega}_3 - n(J_2 - J_1)\omega_1 = -u_3 + w_3 \tag{8c}$$

In the following sections, we will introduce an optimal regional-pole placement technique and a digital redesign technique for systems and observers in a general state space representation.

III. Optimal Regional-Pole Placement

Consider the linear controllable continuous-time system described by

$$\dot{x}_c(t) = Ax_c(t) + Bu_c(t), \qquad x_c(0) \tag{13}$$

where $x_c(t)$ and $u_c(t)$ are an $n \times 1$ state vector and an $m \times 1$ input vector, respectively, and A and B are constant matrices of appropriate dimensions. Let the quadratic cost function for the system in Eq. (13) be

$$J = \int_0^\infty [x_c^T(t)Qx_c(t) + u_c^T(t)Ru_c(t)]\, dt \tag{14}$$

where the weighting matrices Q and R are $n \times n$ non-negative definite and $m \times m$ positive definite symmetric matrices, respectively. The feedback control law that minimizes the performance index in Eq. (14) is given by Ref. 8:

$$u_c(t) = -K_c x_c(t) + E_c r(t) = -R^{-1}B^T P x_c(t) + E_c r(t) \tag{15}$$

where K_c is an $m \times n$ feedback gain, E_c is an $m \times m$ forward gain, $r(t)$ is an $m \times 1$ reference input, and P, an $n \times n$ nonnegative definite symmetric matrix, is the solution of the Riccati equation,

$$PBR^{-1}B^TP - PA - A^TP - Q = 0_n \tag{16}$$

with (Q,A) detectable. The superscript T and the matrix 0_n denote the transpose and an $n \times n$ null matrix, respectively. Thus, the resulting closed-loop system (Fig. 2a) becomes

$$\dot{x}_c(t) = (A - BK_c)x_c(t) + BE_cr(t) \tag{17}$$

The eigenvalues of $(A - BK_c)$, denoted by $\lambda(A - BK_c)$, lie in the open left-half plane of the complex s plane. Our objective is to determine Q, R, and K_c so that the closed-loop system in Eq. (17) has its eigenvalues on or within a specified vertical region. The important results to achieve the desired design are presented in the following.

Theorem 1.[5] Let (A,B) be the pair of the given open-loop system in Eq. (13) with the quadratic cost function in Eq. (14). Also, let α_1 and α_2 with $\alpha_2 > \alpha_1 > 0$ represent the prescribed degrees of relative stability. Then, the eigenvalues of the closed-loop system $(A - BK_c)$ consist of the invariant eigenvalues of A lying to the left of the $-\alpha_1$ vertical line and the other eigenvalues of $(A - BK_c)$ lying within the vertical strip $\{-\alpha_1, -\alpha_2\}$ on the negative real axis in the complex s plane, where $K_c = \gamma R^{-1}B^TP$ with the matrix P being the solution of the Riccati equation:

$$PBR^{-1}B^TP - P(A + \alpha_1 I_n) - (A + \alpha_1 I_n)^TP = 0_n \tag{18a}$$

and the constant gain γ being

$$\gamma = \frac{1}{2} + \frac{\alpha_2 - \alpha_1}{\mathrm{tr}(BK)} \tag{18b}$$

where the matrix I_n is an $n \times n$ identity matrix, $K = R^{-1}B^TP$, and $\mathrm{tr}(\cdot)$ designates the trace of $(\cdot)$. If we choose $\alpha_2 > \max\{|\mathrm{Re}(\lambda_i)|\}$, where $\lambda_i (i = 1, 2, \ldots)$ are the imaginary and pure left-half plane eigenvalues of A, then, all $\lambda(A - BK_c)$ lie inside the vertical strip $\{-\alpha_2, -\alpha_1\}$.

Remark. Theorem 1 will be utilized in Sec. VIII for finding a continuous-time optimal observer. The selection of α_1 in Theorem 1 depends on the prescribed degree of relative stability, whereas the choice of α_2 affects the convergence speed of the estimated states to the exact states and the performance of the designed overall system. For a large value of α_2, the errors of the exact and estimated states will decay quickly; however, the bandwidth of the observer-based overall system will increase. As a result, the overall system will be sensitive to high-frequency disturbances that exist in the practical Space Station. The suitable choices of α_1 and α_2 for the practical Space Station will require several test-bed simulations.

IV. Digital Redesign by Matching of States

Let the continuous-time system be given by

$$\dot{x}_c(t) = Ax_c(t) + Bu_c(t), \qquad x_c(0) \tag{19a}$$

Also, let the associated state-feedback control law be

$$u_c(t) = -K_cx_c(t) + E_cr(t) \tag{19b}$$

where the feedback gain K_c and the forward gain E_c have been given or obtained via the LQR design method developed in Ref. 4. The designed closed-loop system becomes

$$\dot{x}_c(t) = (A - BK_c)x_c(t) + BE_cr(t), \qquad x_c(0) \tag{20}$$

Let the state equation of the digital system that approximates the continuous-time system in Eq. (19a) be represented by

$$\dot{x}_d(t) = Ax_d(t) + Bu_d(kT) \tag{21a}$$

for $kT \le t < (k+1)T$. With the digital control law

$$u_d(kT) = -K_dx_d(kT) + E_dr(kT) \tag{21b}$$

the designed discrete-time closed-loop system becomes

$$\dot{x}_d(t) = Ax_d(t) + B[-K_dx_d(kT) + E_dr(kT)] \tag{22}$$

for $kT \le t < (k+1)T$. A zero-order hold is utilized in Eq. (22). The block diagram representations of the systems in Eqs. (20) and (22) are shown in Figs. 2. Now, the digital redesign problem reduces to finding the state-feedback gain K_d and the forward gain E_d in Eq. (21b) from the state feedback gain K_c and forward gain E_c in Eq. (19b) so that the states of the digital model in Eq. (22) closely match the states of the continuous-time system in Eq. (20) at the sampling instants, for a given $r(t)$.

Assuming $r(t) \approx r(kT)$ over one sampling period, we have the respective discrete-time models of Eqs. (20) and (22) as follows:

$$x_c(kT + T) = Gx_c(kT) - \int_{kT}^{(k+1)T} e^{A(kT+T-\tau)}BK_cx_c(\tau)\,d\tau + HE_cr(kT) \tag{23}$$

and

$$x_d(kT + T) = (G - HK_d)x_d(kT) + HE_dr(kT) \tag{24}$$

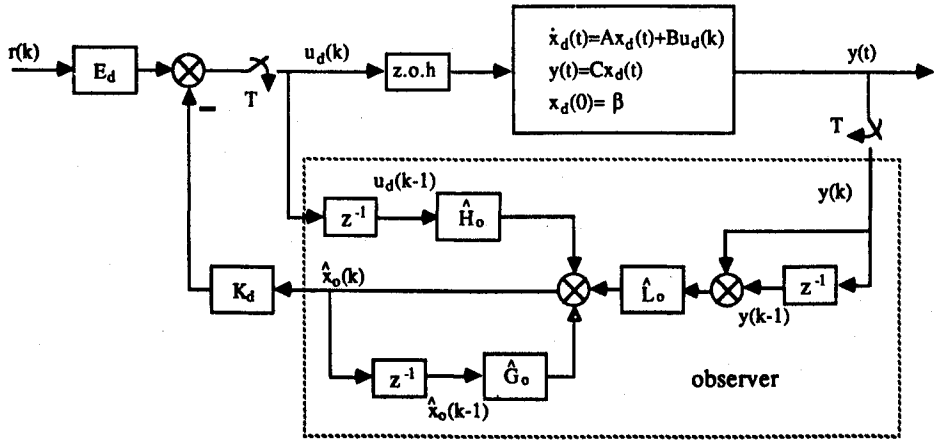

Fig. 3 Block diagram of the redesigned digital observer.

where

$$G \triangleq e^{AT}$$

$$H \triangleq \int_0^T e^{A\tau}B\,d\tau = [G - I_n]A^{-1}B$$

To match the states $x_c(kT)$ in Eq. (23) and $x_d(kT)$ in Eq. (24), we need to approximate the continuous state $x_c(\tau)$ in Eq. (23) by a piecewise-constant state. The block-pulse function,[10] utilized in this paper to approximate the continuous state $x_c(\tau)$, is described in the following.

Let $x_{c_j}(t)$ be the jth element of $x_c(t)$ and be approximated by a set of orthogonal functions $\phi_i(t)$ as

$$x_{c_j}(t) \approx \sum_{i=0}^{\infty} c_i\phi_i(t) \tag{25a}$$

where the block-pulse function is defined as

$$\phi_i(t) = \begin{cases} 1 & \text{for } iT \le t < (i+1)T \\ 0 & \text{otherwise} \end{cases} \tag{25b}$$

The weighting constant c_i can be determined by applying the orthogonal property of the block-pulse functions to Eq. (25a). It is given as

$$c_i = \frac{1}{T}\int_{iT}^{(i+1)T} x_{c_j}(t)\,dt \tag{25c}$$

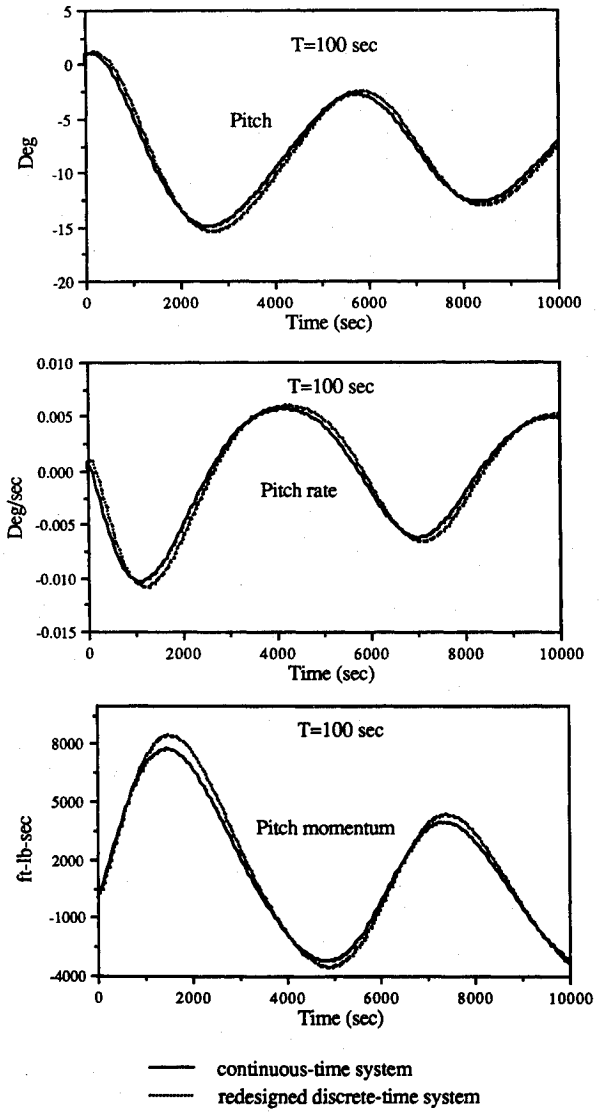

Fig. 4 Pitch axis responses.

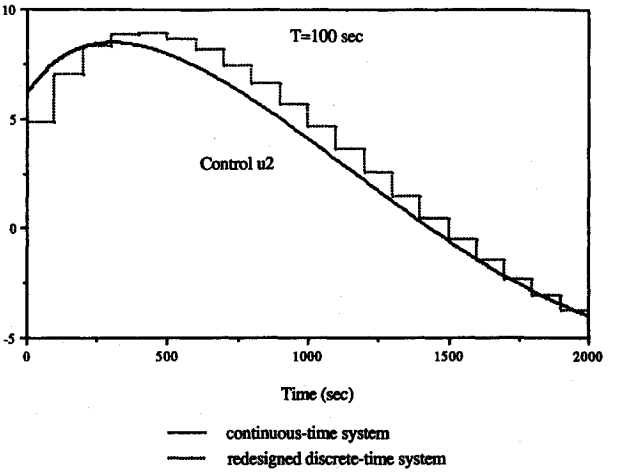

Fig. 5 Pitch control (u_2).

When the curve $x_{c_j}(t)$ is a piece of a straight line in the interval $[iT, (i+1)T]$, then we have

$$c_i = \tfrac{1}{2}[x_{c_j}(iT) + x_{c_j}(iT + T)] \tag{25d}$$

which is the average value of $x_{c_j}(t)$ over the interval $iT \le t \le (i+1)T$. Hence, the continuous-time state $x_c(t)$ can be approximately represented by a piecewise constant state as

$$x_c(t) \approx \sum_{i=0}^{\infty} \frac{1}{2}[x_c(iT) + x_c(iT + T)]\phi_i(t) \tag{26}$$

Using Eq. (26), the integral part in Eq. (23) can be approximated by

$$\begin{aligned}
&\int_{kT}^{(k+1)T} e^{A(kT+T-\tau)}BK_c x_c(\tau)\,d\tau \\
&\approx \int_{kT}^{(k+1)T} e^{A(kT+T-\tau)}BK_c \\
&\times \left\{\sum_{i=0}^{\infty}\frac{1}{2}[x_c(iT) + x_c(iT+T)]\phi_i(\tau)\right\} d\tau \\
&= \int_{kT}^{(k+1)T} e^{A(kT+T-\tau)}BK_c\left\{\frac{1}{2}[x_c(kT) + x_c(kT+T)]\phi_k(\tau)\right\} d\tau \\
&= \int_{kT}^{(k+1)T} e^{A(kT+T-\tau)}B\,d\tau\left(K_c\left\{\frac{1}{2}[x_c(kT) + x_c(kT+T)]\right\}\right) \\
&= HK_c\left\{\frac{1}{2}[x_c(kT) + x_c(kT+T)]\right\}
\end{aligned} \tag{27}$$

where

$$H = \int_{kT}^{(k+1)T} e^{A(kT+T-\tau)}B\,d\tau = (e^{AT} - I_n)A^{-1}B$$

Now, substituting Eq. (27) into Eq. (23) results in

$$x_c(kT + T) = G_c x_c(kT) + H_c r(kT) \tag{28a}$$

where

$$G_c \triangleq (I_n + \tfrac{1}{2}HK_c)^{-1}(G - \tfrac{1}{2}HK_c) \tag{28b}$$

$$H_c \triangleq (I_n + \tfrac{1}{2}HK_c)^{-1}HE_c \tag{28c}$$

Equating the state $x_c(kT)$ in Eq. (28a) to the digital state $x_d(kT)$ in Eq. (24) yields

$$G - HK_d = G_c \qquad HE_d = H_c \tag{29}$$

To solve explicitly for the desired $m \times n$ (nonsquare) feedback gain matrix K_d and $m \times m$ forward gain matrix E_d in Eq. (29), we make use of the following matrix inversion formula[7]:

$$(A + BC^{-1}D)^{-1} = A^{-1} - A^{-1}B(C + DA^{-1}B)^{-1}DA^{-1} \tag{30a}$$

Thus, the matrix $(I_n + \frac{1}{2}HK_c)^{-1}$ in Eq. (28b) can be represented as

$$[I_n + H(2I_m)^{-1}K_c]^{-1} = I_n - H(2I_m + K_cH)^{-1}K_c \tag{30b}$$

Substituting Eq. (30b) into Eq. (28), we have

$$G_c = G - H[\tfrac{1}{2}(I_m + \tfrac{1}{2}K_cH)^{-1}K_c(I_n + G)] \tag{31a}$$

$$H_c = H[(I_m + \tfrac{1}{2}K_cH)^{-1}E_c] \tag{31b}$$

Combining Eqs. (31) and (29), we obtain the desired digital state-feedback gain K_d and forward gain E_d as

$$K_d = \tfrac{1}{2}(I_m + \tfrac{1}{2}K_cH)^{-1}K_c(I_n + G) \tag{32a}$$

$$E_d = (I_m + \tfrac{1}{2}K_cH)^{-1}E_c \tag{32b}$$

If the exact system matrix G and input matrix H in Eqs. (32) are replaced by the bilinear transformation models (i.e., the Tustin approximation models),[2,11] $G \approx [I_n - \frac{1}{2}AT]^{-1}[I_n + \frac{1}{2}AT]$ and $H \approx [I_n - \frac{1}{2}AT]^{-1}BT$, respectively, the resulting digital redesign gains in Eqs. (32) reduce to

$$\bar{K}_d = K_c[I_n - \tfrac{1}{2}(A - BK_c)T]^{-1} \tag{33a}$$

$$\bar{E}_d = (I_m - \tfrac{1}{2}\bar{K}_dBT)E_c \tag{33b}$$

Moreover, to compare the digital redesign gains obtained earlier with those obtained in Ref. 1, we represent the matrices $(I_m + \frac{1}{2}K_cH)^{-1}$ and $G(= e^{AT})$ in Eqs. (32) by a respective infinite series as

$$\left(I_m + \frac{1}{2}K_cH\right)^{-1} = I_m - \frac{1}{2}K_cH + \sum_{j=2}^{\infty}\left(-\frac{1}{2}K_cH\right)^j$$

$$G = e^{AT} = I_n + AT + \sum_{j=2}^{\infty}\frac{1}{j!}(AT)^j$$

When the sampling period T is sufficiently small and $\|K_cH\| < 2$, we can approximate the respective infinite series

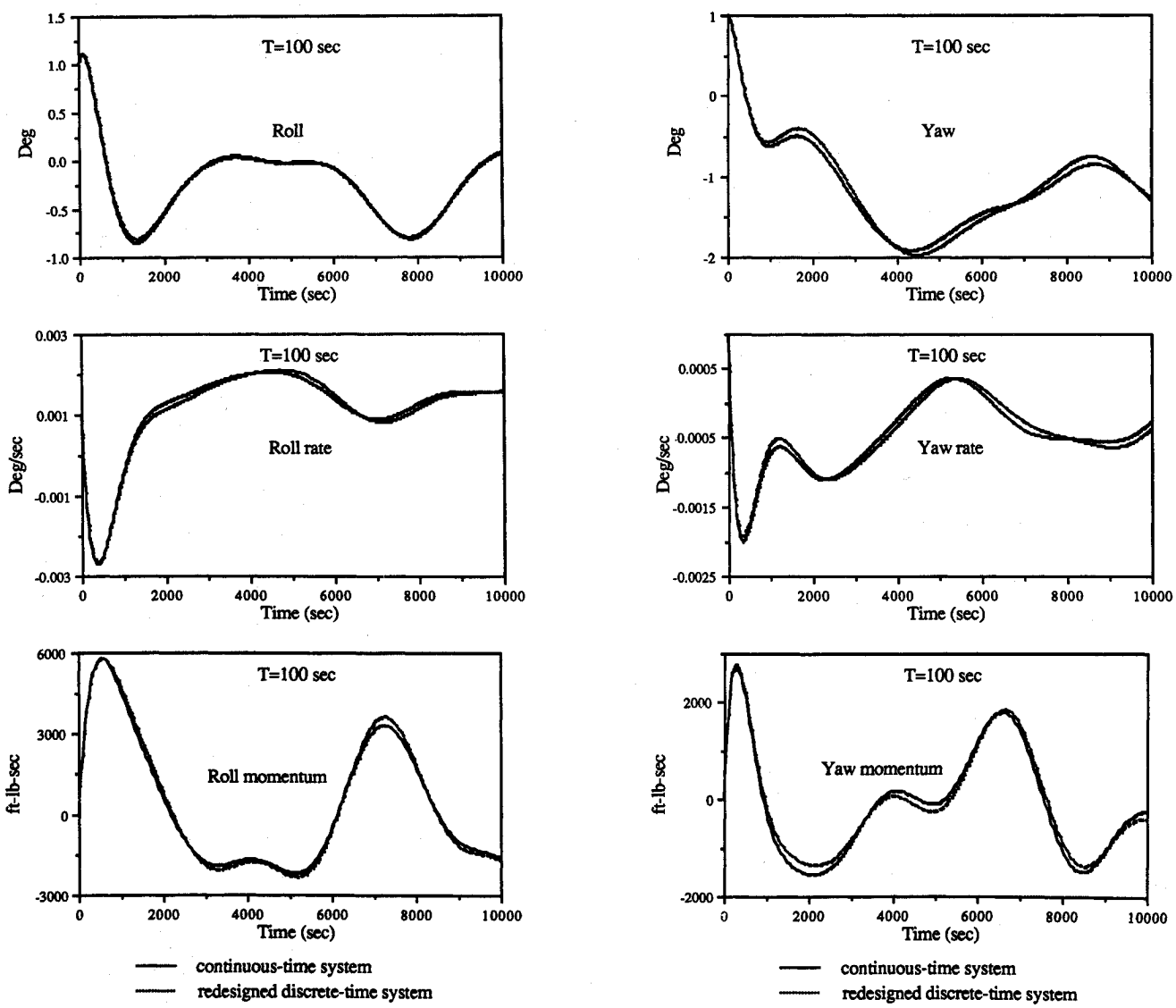

Fig. 6 Roll/yaw axes responses.

by taking the first two terms and substituting them into Eqs. (32) and obtain

$$K_d \approx \tfrac{1}{2}[I_m - \tfrac{1}{2}K_cH]K_c[2I_n + AT]$$

$$= K_c + \tfrac{1}{2}K_c(A - BK_c)T - \tfrac{1}{4}K_cBK_cAT^2$$

$$\approx K_c + \tfrac{1}{2}K_c(A - BK_c)T \triangleq \tilde{K}_d \tag{33c}$$

$$E_d \approx [I_m - \tfrac{1}{2}K_cBT]E_c \triangleq \tilde{E}_d \tag{33d}$$

The approximate gains $\tilde{K}_d$ in Eq. (33c) and $\tilde{E}_d$ in Eq. (33d) are those obtained in Ref. 1.

Remark. A bilinear and inverse bilinear transform method has been utilized in Ref. 7 to derive the same results in Eqs. (32). Also, the comparisons between the $x_d(t)$ in Eqs. (21) and the $x_c(t)$ in Eqs. (19) for the gains in Eqs. (32a) and (32b) and those in Eqs. (33c) and (33d) have been made in Ref. 7. It has been found that the state $x_d(t)$ closely matches the state $x_c(t)$ provided that the sampling period T is properly chosen.

V. New Pseudodigital Observer

Consider the continuous system given in Eq. (19a) with an output function $y(t) \in \Re^{p\times 1}$, i.e.,

$$\dot{x}_c(t) = Ax_c(t) + Bu_c(t) \tag{34a}$$

$$y(t) = Cx_c(t) \tag{34b}$$

The state-feedback control law for the system in Eqs. (34) is given in Eqs. (19), i.e.,

$$u_c(t) = -K_cx_c(t) + E_cr(t) \tag{35a}$$

The closed-loop system becomes

$$\dot{x}_c(t) = (A - BK_c)x_c(t) + BE_cr(t) \tag{35b}$$

When the state $x_c(t)$ is not available, the $x_c(t)$ can be estimated by using the following continuous-time observer[2]:

$$\dot{x}_o(t) = (A - K_oC)x_o(t) + Bu_c(t) + K_oy(t) \tag{36}$$

where $K_o \in \Re^{n\times p}$ is the observer matrix and $x_o(t)$ is the estimate of $x_c(t)$. Hence, the control law in Eq. (35a) can be written as

$$u_c(t) = -K_cx_o(t) + E_cr(t) \tag{37}$$

In this paper, it is desirable to find the matrices $\hat{G}_o$, $\hat{H}_o$, and $\hat{L}_o$ for a new pseudodigital observer

$$\hat{x}_o(k) = \hat{G}_o\hat{x}_o(k-1) + \hat{H}_ou(k-1) + \hat{L}_o[y(k-1) + y(k)] \tag{38}$$

such that

$$\hat{x}_o(k) \approx x_o(t)|_{t=kT} \approx x_c(t)|_{t=kT} \tag{39}$$

Note that for simplicity in notation, the sampling instant T in the discrete-time state equation [Eq. (38)] is dropped. Subtracting Eq. (36) from Eq. (34a) yields

$$\dot{e}_o(t) = (A - K_oC)e_o(t) \tag{40a}$$

where the observer reconstruction error $e_o(t)$ is

$$e_o(t) = x_c(t) - x_o(t) \tag{40b}$$

Table 1 Space Station parameters

Inertial properties, slug-ft^2		Aerodynamic torque, ft-lb
J_{11}	50.28E6	w_1 1 + sin(nt) + 0.5 sin(2nt)
J_{22}	10.80E6	w_2 4 + 2 sin(nt) + 0.5 sin(2nt)
J_{33}	58.57E6	w_3 1 + sin(nt) + 0.5 sin(2nt)
J_{12}	− 0.39E6	
J_{13}	0.16E6	
J_{23}	0.16E6	

Equation (40a) is a dual system of the closed-loop system in Eq. (35b) with $r(t) = 0$, i.e.,

$$\dot{x}_c(t) = (A - BK_c)x_c(t) \tag{41}$$

The digital redesigned system for the system in Eq. (41) has been shown in Eq. (24) with $r(k) = 0$, i.e.,

$$x_d(k+1) = (G - HK_d)x_d(k) \tag{42}$$

where

$$G = e^{AT}$$

$$H = \int_0^T e^{A\tau}B\,d\tau = [G - I_n]A^{-1}B$$

$$K_d = \tfrac{1}{2}(I_m + \tfrac{1}{2}K_cH)^{-1}K_c(I_n + G)$$

Hence, following the dual result of Eqs. (41) and (42), we can write the digital redesigned system for the system in Eq. (40a) as

$$\hat{e}_o(k+1) = (G - \hat{M}\hat{N})\hat{e}_o(k) \tag{43}$$

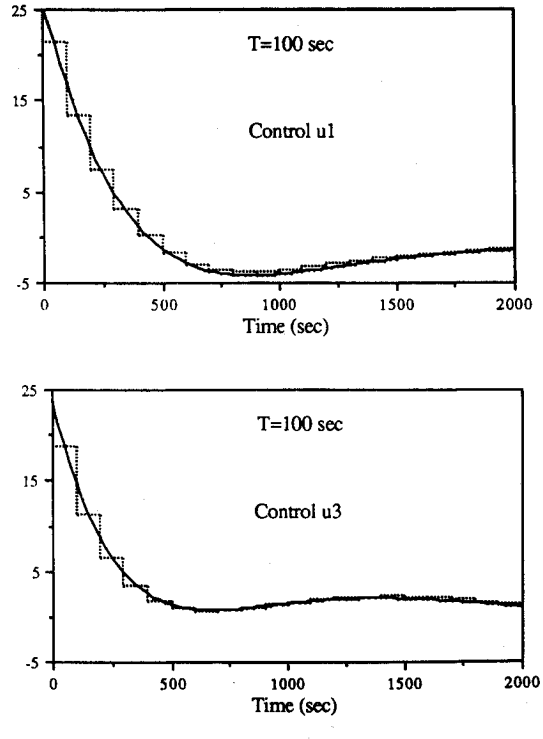

Fig. 7 Roll/yaw controls (u_1 and u_3).

where

$$G = e^{AT}$$

$$\hat{M} = \int_0^T e^{A\tau} K_o \, d\tau = [G - I_n]A^{-1}K_o$$

$$\hat{N} = \tfrac{1}{2}(I_p + \tfrac{1}{2}C\hat{M})^{-1}C(I_n + G)$$

$$\hat{e}_o(k) = x_d(k) - \hat{x}_o(k)$$

Define $\hat{L}_o = \tfrac{1}{2}\hat{M}(I_p + \tfrac{1}{2}C\hat{M})^{-1}$. Equation (43) can be represented as

$$x_d(k+1) - \hat{x}_o(k+1) = [G - \hat{L}_o C(I_n + G)][x_d(k) - \hat{x}_o(k)] \tag{44}$$

Substituting the following identities into Eq. (44):

$$x_d(k+1) = Gx_d(k) + Hu_d(k) \tag{45a}$$

$$y(k) = Cx_d(k) \tag{45b}$$

$$CGx_d(k) = Cx_d(k+1) - CHu_d(k) = y(k+1) - CHu_d(k) \tag{45c}$$

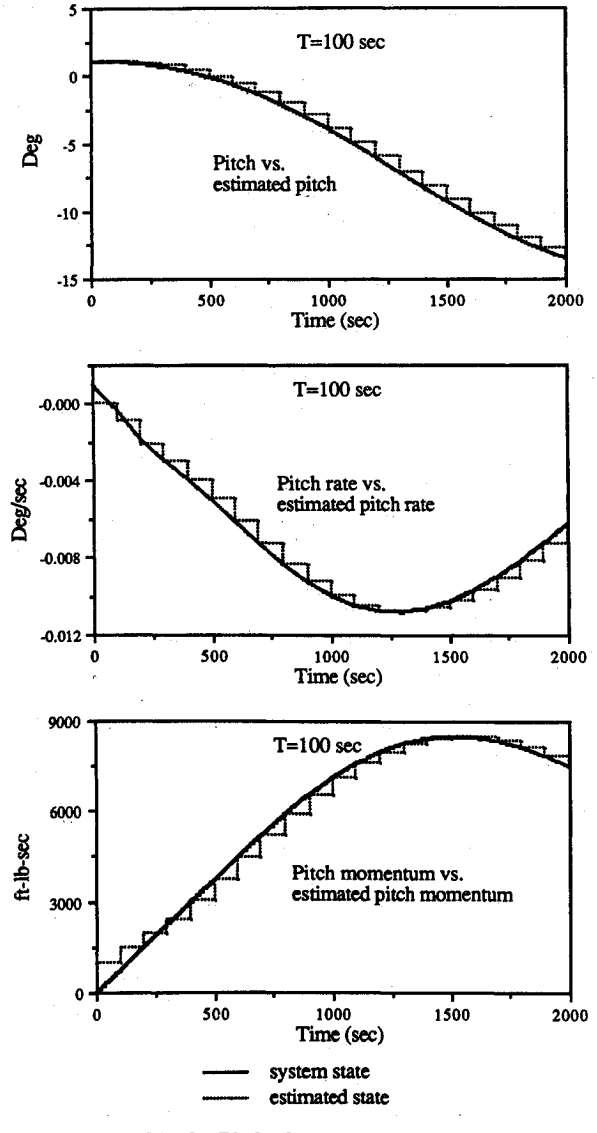

Fig. 8 Pitch observer responses.

we obtain a new pseudodigital observer as

$$\hat{x}_o(k) = \hat{G}_o\hat{x}_o(k-1) + \hat{H}_o u_d(k-1) + \hat{L}_o[y(k-1) + y(k)] \tag{46}$$

where

$$\hat{L}_o = \tfrac{1}{2}[G - I_n]A^{-1}K_o[I_p + \tfrac{1}{2}C(G - I_n)A^{-1}K_o]^{-1}$$

$$\hat{G}_o = G - \hat{L}_o C(I_n + G)$$

$$\hat{H}_o = (I_n - \hat{L}_o C)H$$

Also, the pseudo-state-feedback control law becomes

$$u_d(k) = -K_d\hat{x}_o(k) + E_d r(k) \tag{47}$$

Based on the digital redesign concept in Sec. IV, we observe that the state $x_c(t)$ in Eq. (41) at $t = kT$ closely matches the state $x_d(k)$ in Eq. (42). As a dual result, the state $e_o(t)$ in Eq. (40a) at $t = kT$ would closely match the state $\hat{e}_o(k)$ in Eq. (43), i.e.,

$$e_o(t)|_{t=kT} = x_c(t)|_{t=kT} - x_o(t)|_{t=kT} \approx \hat{e}_o(k) = x_d(k) - \hat{x}_o(k)$$

Since $x_c(t)|_{t=kT} \approx x_d(k)$ and $e_o(t)|_{t=kT} \approx \hat{e}_o(k)$, we have $x_o(t)|_{t=kT} \approx \hat{x}_o(k)$. Also, based on the observer design concept,[2] we observe that the state $x_c(t)$ in Eq. (35b) with $r(t) = 0$ closely matches the estimated state $x_o(t)$ in Eq. (36), i.e., $x_c(t) \approx x_o(t)$. As a result, the states of the continuous-time observer in Eq. (36) at $t = kT$ closely match those of the pseudodigital observer in Eq. (38), i.e.,

$$x_c(t)|_{t=kT} \approx x_o(t)|_{t=kT} \approx x_d(t)|_{t=kT} \approx \hat{x}_o(t)|_{t=kT}$$

The block diagram of the digital redesigned system using the pseudodigital observer in Eq. (46) is shown in Fig. 3.

VI. Digital Control of the Pitch Axis

The pitch axis controller consists of a single input u_2 and four states θ_2, ω_2, h_2, and $\int h_2$. The continuous-time pitch control law is given by

$$u_2 = -K_{A_2}\theta_2 - K_{R_2}\omega_2 - K_{H_2}h_2 - K_{I_2}\int h_2 + E_c r_2(t)$$

$$= -K_c x_c(t) + E_c r_2(t) \tag{48a}$$

where $K_c = [K_{A_2}\ K_{R_2}\ K_{H_2}\ K_{I_2}]$ and $E_c = 1$. Inertial properties of the Phase 1 Space Station are shown in Table 1.[9]

The continuous-time control law gains were computed using the regional-pole assignment method in Ref. 4 with $E_c = I_1$ and are given as follows:

$$K_c = [-2.2022E2 \quad -1.3193E5 \quad -5.5772E-3 \quad -2.0074E-6] \tag{48b}$$

$$E_c = [1.0] \tag{48c}$$

The eigenvalues of the designed closed-loop pitch control system are $(-0.002771, -0.001666, -0.001121, -0.001081)$, which lie within the common region of an open sector, bounded by lines inclined at ± 45 deg from the negative real axis, and the left side of a line at $-0.5n$ (where $n = 0.0011$ rad/s) on the real axis parallel to the imaginary axis in the complex s plane.

The digital redesigned closed-loop system will be of the form shown in Eq. (24) with the digital state feedback gain K_d and forward gain E_d to be determined. Note that the highest critical frequency of the aerodynamic torque is $2n$, where n is the orbital rate of 0.0011 rad/s. Therefore, a

reasonable rule of thumb[3] is to choose the sampling period as $T = [\pi/15(2n)] \approx 100$ s.

For a sampling period of $T = 100$ s, the G and H matrices can be computed. With G, H, and K_c as in Eq. (48b), the gains K_d and E_d can be evaluated from Eqs. (32) and are given as follows:

$$K_d = [-1.7397E2 \quad -1.0422E5 \quad -4.1117E-3 \quad -1.4537E-6] \tag{48d}$$

$$E_d = [7.2419E-1] \tag{48e}$$

The eigenvalues of the digital redesigned closed-loop pitch control system are (0.7605, 0.8466, 0.8860, 0.9031).

The closed-loop response of the pitch system to the aerodynamic disturbance given in Table 1 is shown in Fig. 4. Initial conditions are $\theta_2(0) = 1.0$ deg, $\omega_2(0) = 0.001$ deg/s, and $h_2(0) = 0.0$ ft-lb-s. Simulation results from Ref. 4 for the continuous-time case are included for comparison. Also, the comparison of the continuous-time controller $u_c(t)$ and digital controller $u_d(t)$ is shown in Fig. 5.

VII. Digital Control of the Roll/Yaw Axes

The roll/yaw controller consists of two inputs u_1 and u_3, and eight states including

Roll axis:

$$\theta_1 \quad \omega_1 \quad h_1 \quad \int h_1$$

Yaw axis:

$$\theta_3 \quad \omega_3 \quad h_3 \quad \int h_3$$

The control law is given by:

$$u_1 = -K_{A_1}\theta_1 - K_{R_1}\omega_1 - K_{H_1}h_1 - K_{I_1}\int h_1 - K_{A_3}\theta_3 - K_{R_3}\omega_3 - K_{H_3}h_3 - K_{I_3}\int h_3 + e_{c11}r_1(t) + e_{c12}r_3(t) \tag{49a}$$

$$u_3 = -\bar{K}_{A_1}\theta_1 - \bar{K}_{R_1}\omega_1 - \bar{K}_{H_1}h_1 - \bar{K}_{I_1}\int h_1 - \bar{K}_{A_3}\theta_3 - \bar{K}_{R_3}\omega_3 - \bar{K}_{H_3}h_3 - \bar{K}_{I_3}\int h_3 + e_{c21}r_1(t) + e_{c22}r_3(t) \tag{49b}$$

Let

$$K_c = \begin{bmatrix} K_{A_1} & K_{R_1} & K_{H_1} & K_{I_1} & K_{A_3} & K_{R_3} & K_{H_3} & K_{I_3} \\ \bar{K}_{A_1} & \bar{K}_{R_1} & \bar{K}_{H_1} & \bar{K}_{I_1} & \bar{K}_{A_3} & \bar{K}_{R_3} & \bar{K}_{H_3} & \bar{K}_{I_3} \end{bmatrix}$$

$$E_c = \begin{bmatrix} e_{c11} & e_{c12} \\ e_{c21} & e_{c22} \end{bmatrix}$$

The gains in K_c were computed in Ref. 4 with $E_c = I_2$ and are given as follows:

$$K_c = \begin{bmatrix} -9.5764E2 & -6.1390E5 & -5.5096E-3 & 2.2936E-6 & -1.4405E2 & 2.0593E5 & 4.5858E-3 & 2.590E-6 \\ -3.2524E2 & -1.4063E5 & -1.7273E-3 & -2.6038E-6 & -4.0321E2 & -4.9358E5 & -3.9067E-3 & 8.094E-7 \end{bmatrix}$$

$$E_c = \begin{bmatrix} 1 & 0 \\ 0 & 1 \end{bmatrix}$$

The eigenvalues of the designed closed-loop roll/yaw control system are ($-0.002256 \pm j0.0007756$, $-0.001100 \pm j0.001100$, $-0.001155 \pm j0.0007770$, -0.001100, -0.001099), which lie within the same region as that of the pitch.

As before, we compute the matrices G and H with K_c as in Eqs. (49) and $T = 100$ s. The gains K_d and E_d are computed in Eqs. (32) and are given as follows:

$$K_d = \begin{bmatrix} -7.5318E2 & -4.8030E5 & -4.0006E-3 & 1.7820E-6 & -1.2650E2 & 1.4095E5 & 3.3733E-3 & 1.8354E-6 \\ -2.2794E2 & -8.9085E4 & -1.1377E-3 & -2.1662E-6 & -3.3204E2 & -4.2458E5 & -3.3209E-3 & 5.6773E-7 \end{bmatrix}$$

$$E_d = \begin{bmatrix} 7.2338E-1 & -4.7196E-2 \\ -3.1982E-2 & 8.0376E-1 \end{bmatrix}$$

The eigenvalues of the designed digital system are ($0.7980 \pm j0.06725$, $0.8890 \pm j0.09742$, $0.8883 \pm j0.06916$, $0.8953 \pm j0.0002947$).

The closed-loop response of the roll/yaw system to the aerodynamic disturbance given in Table 1 is shown in Fig. 6. Initial conditions are $\theta_1(0) = \theta_3(0) = 1.0$ deg, $\omega_1(0) = \omega_3(0) = 0.001$ deg/s, and $h_1(0) = h_3(0) = 0.0$ ft-lb-s. It can be seen that the discrete-time states closely match the continuous-time states. The comparison of the continuous-time controller and digital controller is shown in Fig. 7. Note that to show clearly the behavior of transient response between the existing continuous-time controlled system and the proposed discrete-time controlled system, the attitude and momentum time histories of about two orbits are shown in this paper. As the time histories are increased, the responses of the discrete-time controlled system closely match those of the continuous-time controlled system, which is stable.

VIII. Space Station Estimation

A full-order continuous-time observer was constructed for the Space Station in Eqs. (34) using the dual state space equation:

$$\dot{x}_c(t) = A^T x_c(t) + C^T u_c(t) \tag{50}$$

The optimal pole assignment method in Theorem 1 was used to assign the eigenvalues of the observer system $(A - K_oC)$ in the desired vertical strip. Based on the consideration of convergence speed of the estimated states to the exact states, we select the α_1 and α_2 in Theorem 1 for the pitch axis as $\alpha_1 = 0.005$ and $\alpha_2 = 0.02$, respectively. The state space equations of the continuous-time observer are given by

$$\dot{\hat{x}}_o(t) = (A - K_oC)\hat{x}_o(t) + Bu_c(t) + K_oy(t) = A_o\hat{x}_o(t) + Bu_c(t) + K_oy(t) \tag{51a}$$

$$u_c(t) = -K_c\hat{x}_o(t) + E_cr(t) \tag{51b}$$

where $A_o = A - K_oC$.

For the pitch system, the gain K_o in Eq. (51a) is obtained as

$$K_o = \begin{bmatrix} 1.75E-2 & 0.0 \\ 8.75E-5 & 0.0 \\ 0.0 & 8.75E-5 \\ 0.0 & 1.75E-2 \end{bmatrix}$$

where the output matrix C in Eq. (51a) is assumed as

$$C = \begin{bmatrix} 1 & 0 & 0 & 0 \\ 0 & 0 & 0 & 1 \end{bmatrix}$$

The eigenvalues of the designed continuous-time observer for the pitch axis are $(-0.00875 \pm j0.002855,\ -0.00875 \pm j0.003307)$. All designed eigenvalues lie within the specified vertical strip in the s plane.

The redesigned digital observer gains in Eq. (46) are computed as

$$\hat{L}_o = \begin{bmatrix} 5.2343E-1 & 0.0 \\ 2.1529E-3 & 0.0 \\ 0.0 & 2.0896E-3 \\ 0.0 & 5.2239E-1 \end{bmatrix}$$

$$\hat{G}_o = \begin{bmatrix} -4.0205E-2 & 4.7879E1 & 0.0 & 0.0 \\ -4.0560E-3 & 7.9767E-1 & 0.0 & 0.0 \\ 0.0 & 0.0 & 7.9104E-1 & -4.1791E-3 \\ 0.0 & 0.0 & 4.7761E1 & -4.4776E-2 \end{bmatrix}$$

$$\hat{H}_o = \begin{bmatrix} -2.2115E-4 \\ -8.3033E-6 \\ 8.9552E1 \\ 2.3881E3 \end{bmatrix}$$

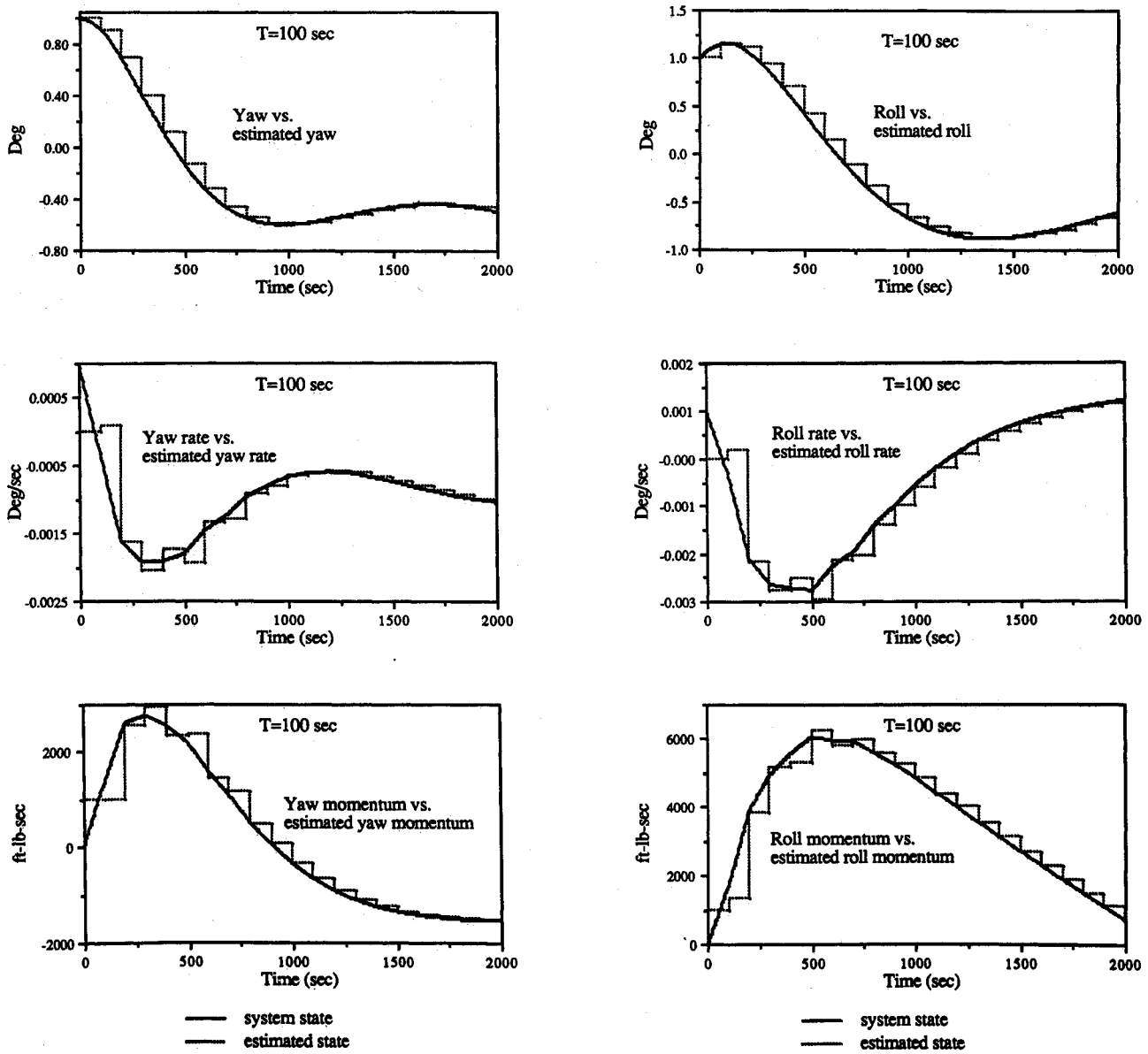

Fig. 9 Roll/yaw observer responses.

The eigenvalues of the redesigned digital observer for the pitch axis are ($0.3787 \pm j0.1367$, $0.3731 \pm j0.1580$).

For the roll/yaw system, the α_1 and α_2 are chosen as $\alpha_1 = 0.04$ and $\alpha_2 = 0.09$, respectively. The observer gain in Eq. (51a) is obtained as

$$K_o = \begin{bmatrix} 9.2506E-2 & 0.0 & 1.4090E-4 & 0.0 \\ 4.6257E-3 & 0.0 & 1.1583E-5 & 0.0 \\ 0.0 & 4.6250E-3 & 0.0 & 5.0875E-5 \\ 0.0 & 9.2500E-2 & 0.0 & 9.4101E-19 \\ 1.4090E-4 & 0.0 & 9.2494E-2 & 0.0 \\ 3.0700E-5 & 0.0 & 4.6243E-3 & 0.0 \\ 0.0 & -5.0875E-5 & 0.0 & 4.6250E-3 \\ 0.0 & 1.2898E-18 & 0.0 & 9.2500E-2 \end{bmatrix}$$

where the output matrix C in Eq. (51a) is assumed as

$$C = \begin{bmatrix} 1 & 0 & 0 & 0 & 0 & 0 & 0 & 0 \\ 0 & 0 & 0 & 1 & 0 & 0 & 0 & 0 \\ 0 & 0 & 0 & 0 & 1 & 0 & 0 & 0 \\ 0 & 0 & 0 & 0 & 0 & 0 & 0 & 1 \end{bmatrix}$$

The selection of the output matrix C in this paper is completely arbitrary. In other words, we assume arbitrarily that the states of the attitude rate are not available for direct measurement due to sensor failure and the states of the CMG momentum are not computable. The eigenvalues of the designed continuous-time observer for the roll/yaw axes are ($-0.04625 \pm j0.05084$, $-0.04625 \pm j0.04884$, $-0.04625 \pm j0.05041$, $-0.04625 \pm j0.04931$). All designed eigenvalues lie within the specified vertical strip in the s plane.

The redesigned digital observer gains in Eq. (46) are computed as

$$\hat{L}_o = \begin{bmatrix} 9.4212E-1 & 0.0 & 3.7751E-3 & 0.0 \\ 1.3536E-2 & 0.0 & -1.3864E-4 & 0.0 \\ 0.0 & 1.3447E-2 & 0.0 & 4.5650E-4 \\ 0.0 & 9.4182E-1 & 0.0 & 1.8660E-3 \\ -2.9783E-3 & 0.0 & 9.4186E-1 & 0.0 \\ 2.7786E-4 & 0.0 & 1.3450E-2 & 0.0 \\ 0.0 & -4.5650E-4 & 0.0 & 1.3447E-2 \\ 0.0 & -1.8660E-3 & 0.0 & 9.4182E-1 \end{bmatrix}$$

$$\hat{G}_o = \begin{bmatrix} -8.8317E-1 & 5.8293 & 0.0 & 0.0 & -1.1364E-3 & 2.4604E-1 & 0.0 & 0.0 \\ -2.6893E-2 & -3.4295E-1 & 0.0 & 0.0 & -1.1991E-3 & -2.5956E-2 & 0.0 & 0.0 \\ 0.0 & 0.0 & -3.4549E-1 & -2.6893E-2 & 0.0 & 0.0 & -9.6619E-3 & -9.1300E-4 \\ 0.0 & 0.0 & 5.8163 & -8.8365E-1 & 0.0 & 0.0 & 1.3343E-1 & -3.7320E-3 \\ -4.5358E-4 & -2.3777E-1 & 0.0 & 0.0 & -8.8375E-1 & 5.8152 & 0.0 & 0.0 \\ 9.1913E-4 & 2.1697E-2 & 0.0 & 0.0 & -2.6849E-2 & -3.4484E-1 & 0.0 & 0.0 \\ 0.0 & 0.0 & 9.6619E-3 & 9.1300E-4 & 0.0 & 0.0 & -3.4549E-1 & -2.6893E-2 \\ 0.0 & 0.0 & -1.3343E-1 & 3.7320E-3 & 0.0 & 0.0 & 5.8163 & -8.8365E-1 \end{bmatrix}$$

$$\hat{H}_o = \begin{bmatrix} -5.7823E-6 & -3.2149E-8 \\ -6.5012E-7 & -1.8807E-8 \\ 3.2716E1 & 7.5052E-1 \\ 2.9093E2 & 1.3387 \\ 5.8789E-8 & -4.9683E-6 \\ 1.9385E-8 & -5.5827E-7 \\ -7.5052E-1 & 3.2716E1 \\ -1.3387 & 2.9093E2 \end{bmatrix}$$

The eigenvalues of the redesigned digital observer are ($-0.5811 \pm j0.3029$, $-0.6463 \pm j0.2789$, $-0.5965 \pm j0.2969$, $-0.6326 \pm j0.2835$).

IX. Discussion of Simulation Results

As an illustration, the pitch axis response of the digital observer to the aerodynamic disturbance given in Table 1 is shown in Figs. 8. The sampling time T remains 100 s. Initial conditions for the Station are $\theta_2(0) = 1.0$ deg, $\omega_2(0) = 0.001$ deg/s, and $h_2 = 0.0$ ft-lb-s. Initial conditions for the observer are set at $\theta_2(0) = 1.0$ deg, $\omega_2(0) = 0.0$ deg/s, and $h_2 = 1000.0$ ft-lb-s, which are different from those of the system.

The digital observer appears to converge very rapidly in the pitch axis. Figure 8 indicates that $\hat{\omega}_2(k)$ and $\hat{h}_2(k)$ converge to steady-state values [i.e., $\omega_2(t)$ and $h_2(t)$] within a few steps. On the other hand, the roll/yaw observer converges at a relatively slower rate. The responses are shown in Fig. 9. Simulation results show that the estimated attitudes and body rates require approximately one orbit to reach steady state. When the sampling period T is selected to be much smaller than 100 s (say, 1 s), the estimated state error will decay quickly at the expense of heavy load on the microprocessors.

X. Conclusions

This paper has presented a digital redesign technique based on matching all of the states of continuous and discrete systems for finding the pseudocontinuous-time regulator with appropriate pole assignment. We have used this technique to obtain a digital momentum management controller for the phase 1 Space Station. In addition, we showed how to redesign a state estimator, again using the Space Station as an example. The states of the planned Space Station are either measurable through sensors or computable via numerical integration techniques. When some states are not accessible for measurement due to sensor failure, the existing state-feedback controller[4,9] can not be implemented. However, the proposed observer-based digital controller can still be implemented for the optimal control of the Space Station. Hence, use of the proposed approach can greatly enhance the reliability of Space Station control. Simulation results have been presented to demonstrate the effectiveness of the proposed technique. Note that achieving the dual goal of continuous-time attitude control and momentum unloading with a multivariable digital controller presented in this paper involves the concept of a torque equilibrium attitude; therefore, relatively large attitude angle fluctuations and biases are to be expected for the real Space Station, operating in real environments.

Acknowledgments

This work was supported in part by the U. S. Army Research Office under Contract DAAL-03-91-G0106 and NASA Johnson Space Center under Grants NAG 9-380 and NAG 9-385. The authors wish to express their gratitude for the valuable remarks and suggestions made by the reviewers.

References

[1]Kuo, B. C., *Digital Control Systems,* Holt, Rinehart and Winston, New York, 1980, pp. 321–338.

[2]Houpis, C. H., and Lammont, G. B., *Digital Control Systems,* McGraw-Hill, New York, 1985.

[3]Åstrom, K. J., and Wittenmark, B., *Computer Controlled Systems—Theory and Design,* Prentice-Hall, Englewood Cliffs, NJ, 1984.

[4]Sunkel, J. W., and Shieh, L. S., "An Optimal Momentum Management Controller for the Space Station," *Journal of Guidance, Control, and Dynamics,* Vol. 13, No. 4, 1990, pp. 659–668.

[5]Shieh, L. S., Dib, H. M., and McInnis, B. C., "Linear Quadratic Regulators with Eigenvalue Placement in a Vertical Strip," *IEEE Transactions on Automatic Control,* Vol. AC-31, No. 3, 1986, pp. 241–243.

[6]Shieh, L. S., Zhang, J. L., and Ganesan, S., "Pseudo-Continuous-Time Quadratic Regulator with Pole Placement in a Specific Region," *IEE Proceedings,* Vol. 137, Pt. D, No. 5, 1991, pp. 297–301.

[7]Tsai, J. S. H., Shieh, L. S., Zhang, J. L., and Coleman, N. P., "Digital Redesign of Pseudo-Continuous-Time Suboptimal Regulators for Large-Scale Discrete Systems," *Control Theory and Advanced Technology,* Vol. 5, No. 1, 1989, pp. 37–65.

[8]Anderson, B. D. O., and Moore, J. B., *Linear Optimal Control,* Prentice-Hall, Englewood Cliffs, NJ, 1971.

[9]Wei, B., Byun, K., Warren, V., Geller, D., Long, D., and Sunkel, J., "A New Momentum Management Controller for the Space Station," *Journal of Guidance, Control, and Dynamics,* Vol. 12, No. 5, 1989, pp. 714–722.

[10]Shieh, L. S., Yeung, C. K., and McInnis, B. C., "Solution of State-Space Equations via Block-Pulse Functions," *International Journal of Control,* Vol. 28, No. 3, 1978, pp. 383–392.

[11]Shieh, L. S., Yates, R. E., and Navarro, J. M., "Representation of Continuous-Time State Equations by Discrete-Time State Equations," *IEEE Transactions on Systems, Man, and Cybernetics,* Vol. SMC-8, No. 6, 1978, pp. 485–492.